



ARTICLE

Pazopanib alleviates neuroinflammation and protects dopaminergic neurons in LPS-stimulated mouse model by inhibiting MEK4-JNK-AP-1 pathway

Hong-yang Sun¹, Jin Wu¹, Rui Wang¹, Shun Zhang¹, Hao Xu¹, Elena Kaznacheyeva², Xiao-jun Lu³, Hai-gang Ren¹ and Guang-hui Wang^{1,4}

Parkinson's disease (PD) is a progressive neurodegenerative disease characterized by the loss of dopaminergic (DA) neurons and the accumulation of Lewy bodies (LB) in the substantia nigra (SN). Evidence shows that microglia-mediated neuroinflammation plays a key role in PD pathogenesis. Using TNF- α as an indicator for microglial activation, we established a cellular model to screen compounds that could inhibit neuroinflammation. From 2471 compounds in a small molecular compound library composed of FDA-approved drugs, we found 77 candidates with a significant anti-inflammatory effect. In this study, we further characterized pazopanib, a pan-VEGF receptor tyrosine kinase inhibitor (that was approved by the FDA for the treatment of advanced renal cell carcinoma and advanced soft tissue sarcoma). We showed that pretreatment with pazopanib (1, 5, 10 μ M) dose-dependently suppressed LPS-induced BV2 cell activation evidenced by inhibiting the transcription of proinflammatory factors iNOS, COX2, IL-1 β , and IL-6 through the MEK4-JNK-AP-1 pathway. The conditioned medium from LPS-treated microglia caused mouse DA neuronal MES23.5 cell damage, which was greatly attenuated by pretreatment of the microglia with pazopanib. We established an LPS-stimulated mouse model by stereotactic injection of LPS into mouse substantia nigra. Administration of pazopanib (10 mg·kg⁻¹·d⁻¹, i.p., for 10 days) exerted significant anti-inflammatory and neuronal protective effects, and improved motor abilities impaired by LPS in the mice. Together, we discover a promising candidate compound for anti-neuroinflammation and provide a potential repositioning of pazopanib in the treatment of PD.

Keywords: Parkinson's disease; neuroinflammation; pazopanib; MEK4-JNK-AP-1 pathway; drug repositioning

Acta Pharmacologica Sinica (2023) 44:1135–1148; <https://doi.org/10.1038/s41401-022-01030-1>

INTRODUCTION

Parkinson's disease (PD) is the second most common neurodegenerative disease and affects more than 1% of the population >65 years old. Epidemiological studies show that PD prevalence is expected to double by 2030 [1, 2]. In the early stage, PD patients show prodromal phenotypes such as rapid eye movement sleep behavior disorder. Subsequently, movement phenotypes, including resting tremor, myotonia and bradykinesia, gradually appear with the development of PD, and psychological or cognitive problems occur at the last stage. These clinical phenotypes are related to the breakdown of the DA system and the occurrence of neuroinflammation [3, 4]. However, the current therapeutic drugs for PD are limited. DA-based therapies focus on stimulating the remaining DA neurons to function but cannot block PD progression. Based on pathogenic mechanism explorations, disease-modifying therapeutic strategies have moved forward in the PD clinic: prevention of the spread and aggregation of pathogenic proteins [5, 6], acceleration of aggregated protein clearance [7, 8], improvements in mitochondrial function [9], and

inhibition of neuroinflammation [10]. Neuroinflammation is a common pathological feature in different subtypes of PD, which leads to the production of neurotoxic factors in various regions and facilitates α -synuclein pathology [11]. Therefore, neuroinflammation is a potential therapeutic target for PD intervention [12]. Despite the difficulties of species differences and side effects in the development of anti-neuroinflammation drugs, three candidates (PMX205, azathioprine, AKST4290) have undergone clinical trials for PD [13].

Neuroinflammation is an immune response characterized by glial hyperactivation in the central nervous system (CNS). Microglia are the first immune effectors to respond to external stimuli to mediate neuroinflammation. When sensing damage-associated molecular patterns (DAMPs) or pathogen-associated molecular patterns (PAMPs), microglia convert to the proinflammatory state, manifesting in proliferation, migration to the injury sites, and release of proinflammatory factors, including TNF- α , interleukin-1beta (IL-1 β), interleukin-6 (IL-6) and prostaglandin E2 (PGE2) [14]. Mild neuroinflammation benefits neuronal repair and maintenance, while

¹Laboratory of Molecular Neuropathology, Jiangsu Key Laboratory of Neuropsychiatric Diseases and College of Pharmaceutical Sciences, Soochow University, Suzhou 215123, China; ²Institute of Cytology of Russian Academy of Sciences, Saint-Petersburg 194064, Russia; ³Department of Neurosurgery, the First People's Hospital of Taicang, Taicang Affiliated Hospital of Soochow University, Suzhou 215400, China and ⁴Center of Translational Medicine, the First People's Hospital of Taicang, Taicang Affiliated Hospital of Soochow University, Suzhou 215400, China

Correspondence: Guang-hui Wang (wanggh@suda.edu.cn)

Received: 5 July 2022 Accepted: 10 November 2022

Published online: 19 December 2022

persistent uncontrolled glial activation and microenvironmental disruption exacerbate neuronal damage and death in aging and neurodegenerative diseases [15]. Thus, neuroinflammation is not only a pathological marker of disease progression but also an important factor aggravating the development of PD.

Microglia-mediated neuroinflammation has critical roles in many neurodegenerative and neuroinflammatory diseases. Studies have shown that blockade of microglial activation by compounds protects neurons from microglia-mediated neuronal death in animal models [16–18]. In MPTP (1-methyl-4-phenyl-1,2,3,6-tetrahydropyridine) PD animal models, the active compounds α -asarone [16] and atractylenolide-1 [17] alleviate MPTP-induced DA neuronal loss and improve animal behaviors. Moreover, both α -asarone and atractylenolide-1 inhibited the LPS-induced activation of BV2 cells, a mouse microglial cell line, suggesting direct inhibitory effects on microglia. In addition, the active compound icariin can inhibit LPS-induced microglial activation *in vitro* and *in vivo* [18]. At the same time, it protects DA against LPS- or 6-OHDA (6-hydroxydopamine)-induced cell death. These studies demonstrate the potential of compounds that target microglia in PD treatment. It has been reported that nonsteroidal anti-inflammatory drugs decrease the risk of PD [19, 20].

Due to the great advantages of drug repositioning, we screened potential anti-inflammatory drugs from an FDA-approved drug library. Among the candidates from screen assays, the vascular endothelial growth factor receptor tyrosine kinase inhibitor (VEGFR-TKI) pazopanib effectively inhibits microglial hyperactivation and protects dopaminergic neurons from neuroinflammation-induced cell death *in vitro* and *in vivo*. Furthermore, pazopanib alleviates LPS-induced neuroinflammation through the MEK4-JNK-AP-1 signaling pathway. Thus, our study demonstrates the potential for the repositioning of pazopanib, which targets microglia, as a promising strategy in PD treatment.

MATERIALS AND METHODS

Experimental animals

Male C57BL/6J mice (6–8 weeks) were purchased from Shanghai SLAC Laboratory Animal (Shanghai, China). All animals were raised in a 12-h light-dark cycle with *ad libitum* access to water and rodent chow. All experiments were approved by the Animal Committee of Soochow University. For drug treatment, all animals were randomly assigned to 4 groups: (1) the solvent + PBS group; (2) the pazopanib + PBS group; (3) the solvent + LPS group; and (4) the pazopanib + LPS group. Mice in group (2) and group (4) were administered pazopanib (10 mg/kg per day) using intraperitoneal injection for ten consecutive days. Mice in the other groups were administered an equal volume of solvent. The solvent contained 10% DMSO and 90% corn oil. On day 10, mice were treated with LPS (2 μ g) or an equal volume of PBS by using stereotaxic injection at AP -3.3 mm, ML ± 1.2 mm, DV -4.6 mm from bregma. All animals were treated with pazopanib or solvent for another 7 days. Twenty-four hours after completing all treatments, the animals were sacrificed for immunocytochemistry staining. General anesthesia was induced with intraperitoneal injection of pentobarbital sodium at a dose of 40 mg/mL (RWD Life Science Co., Shenzhen, Guangdong, China). Pazopanib and LPS were purchased from MedChemExpress (Monmouth Junction, NJ, United States). All animal experiments were carried out according to the institutional guidelines for the use and care of animals, and all procedures were approved by the ethical committee of Soochow University.

Behavioral experiments

We performed behavioral tests to evaluate fine motor coordination and balance, including the pole test, beam walking test, rotarod test and open field test. The behavioral instruments were purchased from SANS Biological Technology, Nanjing, China. All motor assessments were performed in identical animal facilities.

Animal training and test methods were performed according to previous studies [21–24].

Pole test. A 50 cm high, 1 cm in diameter, rough-surfaced wood pole was placed into the home cage. On the training day, each mouse was placed on the top of the pole and allowed to crawl downward from the top to the home cage three times. On the test day, each mouse was placed head-down on the top of the pole and the time taken to descend back into the cage was recorded. The experiment was repeated three times for each mouse and the average times were analyzed.

Beam walking test. The apparatus consisted of a 50 cm length, 5 cm width plastic beam that was 50 cm above the floor with a 10 cm³ enclosed box at the end of the beam. On the training day, each mouse was placed at the initial 20 cm of the beam and was trained to cross the beam to the enclosed box. On the test day, the number of hind-limb slips of each mouse was calculated. The experiment was repeated three times for each mouse and the average times were analyzed.

Rotarod test. On the training day, each mouse was placed on the rotarod and trained until it was able to remain on the rotarod for more than 2 min at a speed of 4 revolutions per minute (r/min). On the test day, the speed of the rotarod was accelerated from 4 r/min to 40 r/min in 5 min. Each mouse was allowed to walk freely on the rotarod, and the latency time to fall was recorded. The experiment was repeated three times for each mouse.

Open field test. A square arena (40 cm \times 40 cm \times 40 cm) was divided into 16 equal-sized squares and the 4 squares in the center were defined as the center area. The mouse was placed in the corner of the square arena and video recorded for 15 min. The travel distance in the center area of each mouse was analyzed.

Cell culture and drug treatment

All cells were cultured in a humidified incubator at 37 °C with 5% CO₂. BV2 cells were grown in Dulbecco's modified Eagle's medium (DMEM) (Gibco, Grand Island, NY, USA) with 10% heat-inactivated fetal bovine serum (FBS), penicillin (100 μ g/mL), and streptomycin (100 μ g/mL).

Primary cultured microglia were isolated from 3-day-old C57BL/6J mice. In brief, the brain tissue was removed from neonatal mice, and the meninges and blood vessels were stripped, digested and filtered to obtain a mixed cell suspension. Finally, the cells were plated on 75 cm² culture flasks coated with poly-D-lysine and cultured with DMEM/F12 supplemented with 10% heat-inactivated FBS and the antibiotics mentioned above. Microglia were harvested after 2 weeks of culture by gently shaking the flasks and were replated onto the indicated plates. Seeded cells were prepared for subsequent dosing treatments. Pazopanib and LPS were purchased from MedChemExpress (Monmouth Junction, NJ, United States).

siRNA assay

JNK siRNAs were purchased from GenePharma (Shanghai, China) with the following sequences: *si-NC* sense: 5'-AUGGCAUCAUAGCUGCAC-3'; *si-JNK* sense: 5'-UGAUUCAGAUUGAGUUAGA-3' [25]. The siRNA was performed with Lipofectamine RNAiMAX Transfection Reagent (Invitrogen, USA) according to the manufacturer's instructions. BV2 cells were transfected with 2 μ M siRNA for 24 h, and then the siRNA was removed. BV2 cells were cultured for another 24 h, treated with pazopanib or DMSO for 4 h and then stimulated with LPS or PBS for 20 h. The cells were collected for further assays.

Cell viability assay

Cell viability was detected with a Cell Counting Kit-8 (APExBio Technology LLC, Houston, USA) according to the manufacturer's instructions. In brief, cells were pretreated with various compounds (10 μ M) or varying doses (0, 1, 5, 10 μ M) of pazopanib for 4 h and then

treated with LPS (1 µg/mL) for another 20 h. The cells were incubated with 10% CCK8 reagent at 37 °C for 3 h. The absorbance was detected at 450 nm by a microplate reader to determine cell viability.

ELISA

For the screening assays, BV2 cells were subjected to small-molecule compounds from an FDA-approved drug library for 4 h, followed by LPS stimulation for another 20 h. The compounds were excluded if they led cells to a poor condition or death. The culture media were corrected and subjected to ELISAs to detect TNF-α with a kit (BOSTER, Wuhan, China), which was described previously [26]. The details of the small-molecule compounds are available on the following website: https://www.medchemexpress.cn/screening/FDA-approved_Drug_Library.html.

For the detection of TNF-α, PGE2 and IL-6, the culture media were subjected to ELISAs with ELISA kits (BOSTER, Wuhan, China).

Quantitative Real-Time PCR (qRT-PCR)

Total cellular RNA was extracted using a TRIzol commercial kit (Invitrogen, Carlsbad, CA, USA) according to the protocol described previously [27, 28]. RNA was reverse-transcribed into cDNA with HiScript II Q RT SuperMix (Vazyme Biotech, Nanjing, China). Quantitative real-time PCR analysis was implemented on an ABI 7500 PCR instrument (Applied Biosystems, Carl) with a SYBR green kit (Takara, Carlsbad, CA, USA). The sequences of the primers used were as follows: mouse *iNOS* sense: 5'-TCCCAGCTGCCCTTCAAT-3' and 5'-CGGATCTCTCCTCCTGGG-3'; mouse *COX2* sense: 5'-CAGGCTGAACCTCGAAACA-3' and 5'-GCTCAGAGGCCACTGATACCTA-3'; mouse *TNF-α* sense: 5'-CATCTTCTCAAATTCGAGTGACAA-3'; and 5'-CTAGGTTTGGCGAGTAGATC-3'; mouse *IL-6* sense: 5'-GCTATGAAGTTCTCTCTGC-3' and 5'-CTAGGTTTGGCGAGTAGATC-3'; mouse *IL-1β* sense: 5'-TGGCAACTGTCTCTG-3' and 5'-GGAAGCAGCCCTTCACTTTT-3'; mouse *β-actin* sense: 5'-GACTGACTGACTACCTC-3' and 5'-GACAGCGAGGCCAGGATG-3'. The relative mRNA expression level was calculated by the $2^{-\Delta\Delta CT}$ method and quantified and normalized to *β-actin*.

Immunoblot analysis and antibody information

BV2 cells or primary microglia were collected and lysed in cell lysis buffer, and the cell lysate was boiled with an equal volume of loading buffer to denature the samples. Equal amounts of protein samples were separated in SDS-PAGE gels and transferred to PVDF membranes (Millipore). The PVDF membranes were blocked with 5% skimmed milk and probed with primary antibodies. Immunoblot analyses were performed with the following primary antibodies: anti-iNOS, anti-COX2, anti-Histone 2B, anti-NF-κB/p65, anti-IκBα and anti-tubulin (Abcam, Cambridge, MA, USA); anti-c-Fos, anti-c-Jun, anti-phospho-c-Jun (Ser73), anti-phospho-c-Fos (Ser32), anti-phospho-p65, anti-SAPK/JNK and anti-phospho-SAPK/JNK (Thr183/185) (Cell Signaling Technology, Danvers, MA, USA); and anti-phospho-Erk1/2, anti-ERK1, anti-p38, anti-phospho-p38 and anti-β-actin (Santa Cruz Biotechnology, Santa Cruz, CA, USA). The membranes were incubated with the indicated primary antibodies overnight. They were then incubated with goat anti-mouse or anti-rabbit IgG-HRP secondary antibodies (Thermo Fisher Science, Waltham, MA, USA) for 2 h. The proteins were visualized using an ECL detection kit (Thermo Fisher).

Subcellular fractionation assay

Fractionation assays were performed as described previously [29]. In brief, BV2 cells were treated with pazopanib for 4 h, treated with LPS for 15 min, and harvested immediately with fractionation buffer + NP40 buffer (320 mM sucrose, 3 mM CaCl₂, 320 mM MgAc, 0.1 mM EDTA, 1 mM DTT, 0.5 mM PMSF, and 0.5% NP40 in ddH₂O) on ice. After cryogenic centrifugation, the nuclear fractions are precipitated, and cytoplasmic components are in the supernatant. The precipitate was washed with NP40 buffer and lysed with cell lysate buffer (50 mM Tris pH 7.6, 150 mM NaCl,

0.5% deoxycholate sodium, 1% NP40, with a protease inhibitor cocktail (Roche) in ddH₂O). Histone 2B (H2B) served as a nuclear marker, and tubulin served as a cytoplasmic marker.

Immunofluorescence staining

BV2 cells were fixed in 4% paraformaldehyde (PFA), permeabilized with 0.1% Triton X-100 for 10 min, and blocked with 2% FBS in PBS for another 10 min. Immunofluorescence staining was performed with the primary antibody anti-p65 (Santa Cruz Biotechnology, Santa Cruz, CA, USA). Primary antibodies were incubated in blocking buffer at 4 °C overnight. Then, they were incubated with Alexa Fluor secondary antibodies (Thermo Fisher Science, Waltham, MA, USA) for 2 h at room temperature. DAPI (Sigma, St Louis, MO, USA) was used for nuclear counterstaining as described previously [30]. Finally, the cells were observed with an inverted IX71 microscope system (Olympus, Tokyo, Japan).

The positive cells were counted and analyzed using Fiji software (National Institutes of Health, Bethesda, MD, USA).

Propidium iodide (PI) staining assay

MES23.5 cells were treated with varying microglial conditioned media for 24 h. Then, the cells were incubated with Hoechst 33342 (Sigma, St. Louis, MO, USA) and PI (Sigma, St. Luis, MO, USA) for 10 min. The cells were imaged with an inverted IX71 microscope system (Olympus, Tokyo, Japan). The positive cells were counted and analyzed using Fiji software (National Institutes of Health, Bethesda, MD, USA).

Immunohistochemistry and imaging

After all treatments, the animals were anesthetized with pentobarbital sodium at a dose of 40 mg/mL by intraperitoneal injection and transcranially perfused with 20 mL PBS, followed by 20 mL 4% PFA in 0.1 M PBS (pH 7.4). The brains were removed and postfixed in the same fixation agent at 4 °C for 3 d, followed by 30% sucrose for another 3 d. The brains were cut into 20 µm-thick slices using a freezing microtome (Leica CM1950, Leica Biosystems, Nussloch, DEU). The immunocytochemistry staining was performed with primary antibodies: anti-TH (Santa Cruz Biotechnology, Santa Cruz, CA, USA), anti-IBA1 (Wako Chemicals, Japan), and anti-GFAP (Millipore, Billerica, MA, USA) at 4 °C overnight. Then, the slices were incubated with Alexa Fluor secondary antibodies for 2 h at room temperature. Finally, the slices were stained with DAPI for 10 min to mark the nucleus. All slices were imaged with an inverted IX71 microscope system (Olympus, Tokyo, Japan). Three slices for each of the three animals were taken into statistical analysis. The fluorescence intensities of TH, IBA1, and GFAP were analyzed using FIJI software (National Institutes of Health, Bethesda, MD, USA) as described previously [31].

Statistical analysis

Photoshop 7.0 (Adobe, San Jose, CA, USA) was used for results quantification, and GraphPad Prism 7.00 (GraphPad Software, Version X; La Jolla, CA, USA) was used for statistical analysis and graphing. All data are presented as the mean values ± standard errors of the means (SEM). Statistical significance was determined using one-way analysis of variance (ANOVA) followed by Dunnett's multiple-comparisons test. *P* values lower than 0.05 were considered statistically significant.

RESULTS

Identification of VEGFR-TKIs as potential anti-inflammatory factors TNF-α is one of the most prominent proinflammatory cytokines involved in inflammation amplification and secondary neuron damage. Multiple types of TNF-α blockers have been successful in alleviating a number of inflammatory conditions [32, 33]. Using TNF-α as an indicator for BV2 activation, we screened a small molecular compound library composed of FDA-approved drugs for compounds that can inhibit LPS-induced BV2 activation (Fig. 1a). We identified 77

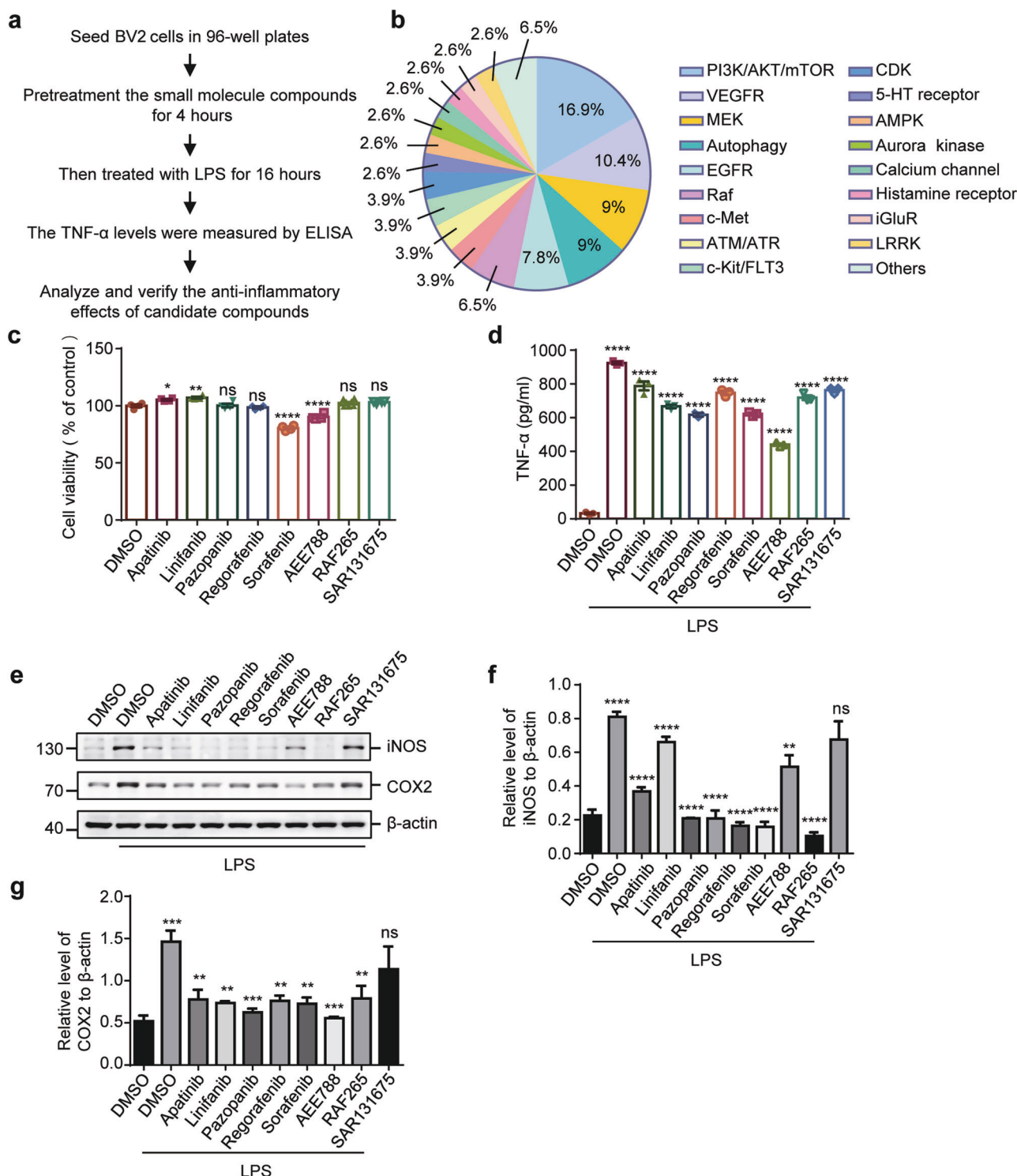


Fig. 1 Anti-neuroinflammatory small molecule compound screening and validation. **a** The workflow for screening anti-neuroinflammatory small molecule compounds. **b** Classification of anti-inflammatory candidates by targets. **c** Anti-inflammatory effect validation of VEGFR-TKIs by ELISA and immunoblot analysis. BV2 cells were treated with TKIs (10 μM) or DMSO for 4 h and then treated with LPS (1 μg/ml) or PBS for 20 h. Cell viability of the BV2 cells treated with VEGFR-TKIs for 24 h was measured by CCK8 assay. The values are presented as the mean ± SEM from three independent experiments. **P* < 0.05, ***P* < 0.01, *****P* < 0.0001, ns, no significant difference vs. the LPS group, one-way ANOVA followed by Dunnett's multiple-comparisons test. **d** BV2 cells were treated as in **c**. TNF-α levels were measured using ELISA. The values are presented as the mean ± SEM from three independent experiments. *****P* < 0.0001 vs. the LPS group, one-way ANOVA followed by Dunnett's multiple-comparisons test. **e** BV2 cells were treated as in **c**. After treatment, BV2 cells were collected, lysed and subjected to immunoblot analyses with the indicated antibodies against iNOS, COX2, or actin. **f, g** The quantification of the intensity of iNOS (**f**) and COX2 (**g**) relative to actin is shown. The values are presented as the mean ± SEM from three independent experiments. ***P* < 0.01, ****P* < 0.001, *****P* < 0.0001, ns, no significant difference vs the LPS group, one-way ANOVA followed by Dunnett's multiple-comparisons test.

Table 1. The candidates of anti-inflammatory small molecular compounds

Targets	Small molecular compounds		
PI3K/AKT/mTOR	A66	Alpelisib	Apitolisib
	AS-604850	AZD5363	AZD6482
	CCT128930	HS-173	Idelalisib
	PIK-294	PIK-93	Rapamycin
	Tricirbine		
VEGFR	AEE788	Apatinib	Linifanib
	Pazopanib	RAF265	Regorafenib
	SAR131675	Sorafenib	
MEK	Binimetinib	PD0325901	PD318088
	Pimasertib	Refametinib	Selumetinib
	Trametinib		
Autophagy	Aliskiren	Ezetimibe	Lomustine
	Megestrol	Raloxifene	Silibinin
	Topotecan		
EGFR	Afatinib	Daphnetin	Rociletinib
	Sapitinib	TAK-285	Varlitinib
Raf	AZ 628	CEP-32496	Dabrafenib
	TAK-632	Vemurafenib	
ATM/ATR	Chloroquine Phosphate	ETP-46464	Schisandrin B
c-Met	Cabozantinib	AMG 337	BMS-777607
c-Kit/FLT3	Amuvatinib	TCS 359	Tyrphostin AG 1296
Cyclin dependent kinase (CDK)	LDC000067	PHA-793887	TG003
5-HT receptor	Alprenolol	Ramosetron	
AMPK	HTH-01-015	WZ4003	
Aurora kinase	Alisertib	Barasertib	
Calcium channel; CaSR	Cinacalcet	Clevidipine	
Histamine Receptor	Antazoline	Famotidine	
iGluR	Ifenprodil	Procyclidine	
LRRK2	GNE-0877	GNE-9605	
Others	Benzylamine	BIO	Hexylresorcinol
	Ibrutinib	Isoconazole	

candidates with significant anti-inflammatory effects from 2471 compounds (Table S1). We classified these candidates into 18 categories according to their targets. Among the positive drugs, the top three categories were associated with the PI3K/AKT/mTOR signaling pathway, the VEGFR signaling pathway and the MEK signaling pathway (Fig. 1b and Table 1). As the anti-inflammatory effects of the PI3K/AKT/mTOR signaling pathway have been well studied, we chose VEGFR-TKI candidates for further identification. We examined the effects of these eight VEGFR inhibitors on cell viability and LPS-induced activation in BV2 cells. Among the VEGFR-TKI candidates, we found that four compounds (pazopanib, regorafenib, RAF265, and SAR131675) had no toxic effects at a concentration of 10 μ M (Fig. 1c). All compounds had significant inhibitory effects on the production of TNF- α by BV2 cells that were treated with LPS, especially pazopanib (Fig. 1d). Moreover, immunoblot analyses also showed that most of the candidates had inhibitory effects on LPS-induced BV2 activation, which was indicated by the decreases in inducible nitric oxide synthase (iNOS) (Fig. 1e, f) and cyclooxygenase-2 (COX2) (Fig. 1e, g).

Pazopanib suppressed proinflammatory factor production in BV2 cells and microglia

Among all VEGFR-TKI candidates, pazopanib showed strong anti-inflammatory effects; thus, we chose it as a representative drug for further identification. Since pazopanib is an anticancer agent with certain cytotoxicity [34], we examined the dose-dependent effects of pazopanib on cell viability. In BV2 cells, the cell viability was decreased when the concentration of pazopanib reached 20 μ M with PBS as the solvent control (Fig. 2a). We found that no changes in cell viability were observed at concentrations up to 20 μ M in LPS-treated BV2 cells (Fig. 2a). We also examined the toxicities of pazopanib to astrocytes (mouse astrocyte type I clone C8D1A) and DA neurons (mouse DA neuronal cell line MES23.5). Pazopanib did not affect the viability of these two types of cells at doses up to 20 μ M (Fig. S1a, b). Thus, we chose doses of pazopanib lower than 10 μ M for further identification. In BV2 cells that were treated with different doses of pazopanib, dose-dependent decreases in iNOS and COX2 by pazopanib were observed in BV2 cells that were treated with LPS (Fig. 2b–d). In addition, pazopanib also decreased iNOS and COX2 levels in primary microglia that were treated with LPS (Fig. 2e–g).

We further examined the effects of pazopanib on the production of some proinflammatory factors. In a dose-dependent manner, pazopanib inhibited the production of TNF- α , prostaglandin E2 (PGE2) and interleukin 6 (IL-6) by BV2 cells that were stimulated with LPS, which was determined using ELISAs (Fig. 3a–c). Furthermore, pazopanib pretreatment repressed the transcription of *iNOS*, *COX2*, *Il-1 β* , and *Il-6* in BV2 cells that were treated with LPS (Fig. 3d–g). Thus, the data suggest that pazopanib represses microglial activation.

The anti-inflammatory effect of pazopanib is independent of the NF- κ B pathway

It is well known that the transcription of inflammatory factors is mainly regulated by several key transcription factors, including nuclear factor kappa B (NF- κ B), activator protein (AP-1), activated T-cell nuclear factor (NFATs), and signaling and transcriptional activator proteins (STAT) [35–38]. As the NF- κ B pathway in inflammation has been the most documented, we wondered whether the NF- κ B pathway is influenced by pazopanib. When TLR4 is activated by LPS, cytosolic I κ B α is phosphorylated and then degraded through the ubiquitination-proteasomal pathway, which releases the partner NF- κ B, leading to the translocation of NF- κ B into the nucleus [29]. In BV2 cells that were treated with pazopanib, the nuclear translocation of NF- κ B/p65 was not influenced after the cells were stimulated by LPS (Fig. 4a–d). Furthermore, the degradation of I κ B α and the phosphorylation of I κ B α or NF- κ B/p65 were not changed by pazopanib in BV2 cells that were treated with LPS (Fig. 4e, f). Thus, the data suggest that the anti-inflammatory effects of pazopanib do not depend on the NF- κ B pathway.

Pazopanib alleviates LPS-induced inflammation through the MEK4-JNK-AP-1 pathway

We next examined the influence of pazopanib on the AP-1 pathway. During inflammatory responses, the activation of the mitogen-activated protein kinases (MAPKs) that include extracellular signal-regulated kinase (ERK), c-Jun N-terminal kinase (JNK) and p38 promotes the expression and phosphorylation of c-Jun and c-Fos that form AP-1 dimers and induce the transcription of proinflammatory proteins [39]. In our observations, the phosphorylation of JNK was increased after BV2 cells were stimulated with LPS (Fig. 5a, b). However, the LPS-induced phosphorylation of JNK was decreased if BV2 cells were treated with pazopanib (Fig. 5a, b). Furthermore, both the protein levels and phosphorylation levels of c-Jun and c-Fos were significantly elevated (Fig. 5a, b), suggesting activation of the AP-1 signal. The phosphorylation of other MAPKs, ERK, and p38, was also increased

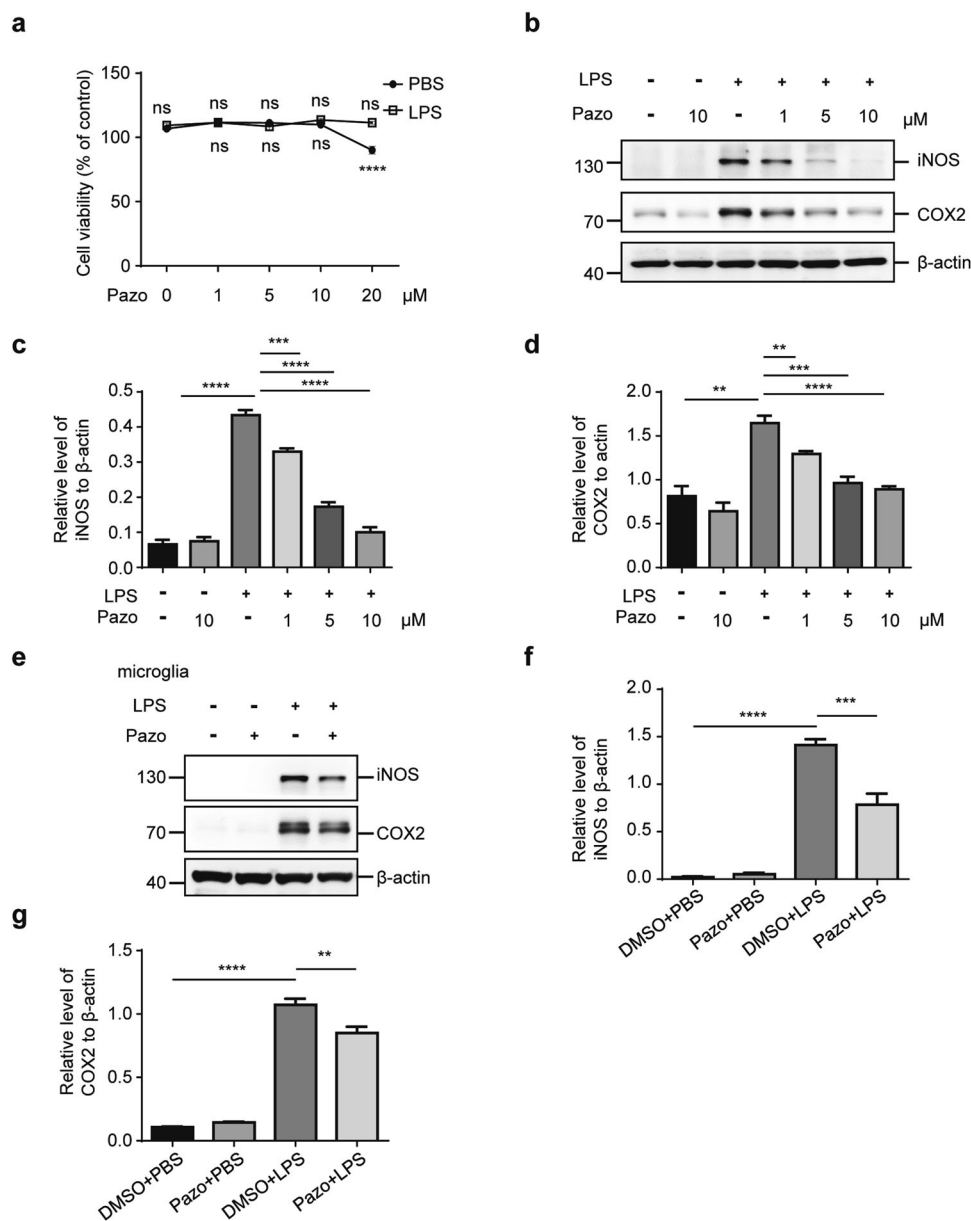


Fig. 2 Pazopanib inhibits LPS-induced activation of BV2 cells **a** BV2 cells were pretreated with pazopanib (0, 1, 5, 10, 20 μM) or DMSO for 4 h and then exposed to LPS (1 μg/mL) or PBS for 20 h. Cell viability was measured by CCK8 assay. The values are presented as the mean ± SEM from three independent experiments. **** $P < 0.0001$, ns no significant difference vs. the DMSO group, one-way ANOVA followed by Dunnett's multiple-comparisons test. **b–d** BV2 cells were pretreated with pazopanib (0, 1, 5, 10, 20 μM) or DMSO for 4 h and then exposed to LPS (1 μg/mL) or PBS for 20 h. The protein levels of iNOS, COX2, and actin were measured using immunoblot analysis (**b**). The quantification of the intensities of iNOS (**c**) and COX2 (**d**) relative to actin are shown. The values are presented as the mean ± SEM from three independent experiments. ** $P < 0.01$, *** $P < 0.001$, **** $P < 0.0001$, ns, no significant difference vs. the LPS group, one-way ANOVA followed by Dunnett's multiple-comparisons test. **e–g** Primary microglia were pretreated with pazopanib (5 μM) or DMSO for 4 h and then exposed to LPS (1 μg/mL) or PBS for 20 h. The protein levels of iNOS, COX2, and actin were measured using immunoblot analyses (**e**). The quantification of the intensity of iNOS (**f**) and COX2 (**g**) relative to actin is shown. The values are presented as the mean ± SEM from three independent experiments. ** $P < 0.01$, *** $P < 0.001$, **** $P < 0.0001$, one-way ANOVA followed by Dunnett's multiple-comparisons test.

after BV2 cells were stimulated with LPS, but pazopanib treatment did not influence the phosphorylation of these two kinases (Fig. 5c, d). To further confirm the involvement of JNK in pazopanib-induced anti-inflammatory effects, we used siRNA to knock down JNK in LPS-stimulated BV2 cells that were treated with or without pazopanib. In BV2 cells without JNK knockdown, pazopanib significantly decreased LPS-induced iNOS and COX2 levels (Fig. 5e, f). In BV2 cells in which JNK was knocked down, LPS-induced iNOS and COX2 expression was decreased compared to that in BV2 cells without JNK knockdown (Fig. 5e, f). Moreover,

LPS-induced iNOS and COX2 expression was not significantly changed by pazopanib in BV2 cells in which JNK was knocked down (Fig. 5e, f). Thus, the data suggest that the anti-inflammatory effects of pazopanib depend on JNK signaling.

JNK is regulated by upstream mitogen-activated protein kinases (MAPKKs, also named MEKs), including mitogen-activated protein kinase kinase 4 (MEK4) and MEK7 [40]. In BV2 cells that were treated with LPS, the phosphorylation of MEK4 but not MEK7 was increased (Fig. 5g, h). In addition, pazopanib treatment alleviated the phosphorylation of MEK4 (Fig. 5g, h). Thus, our data

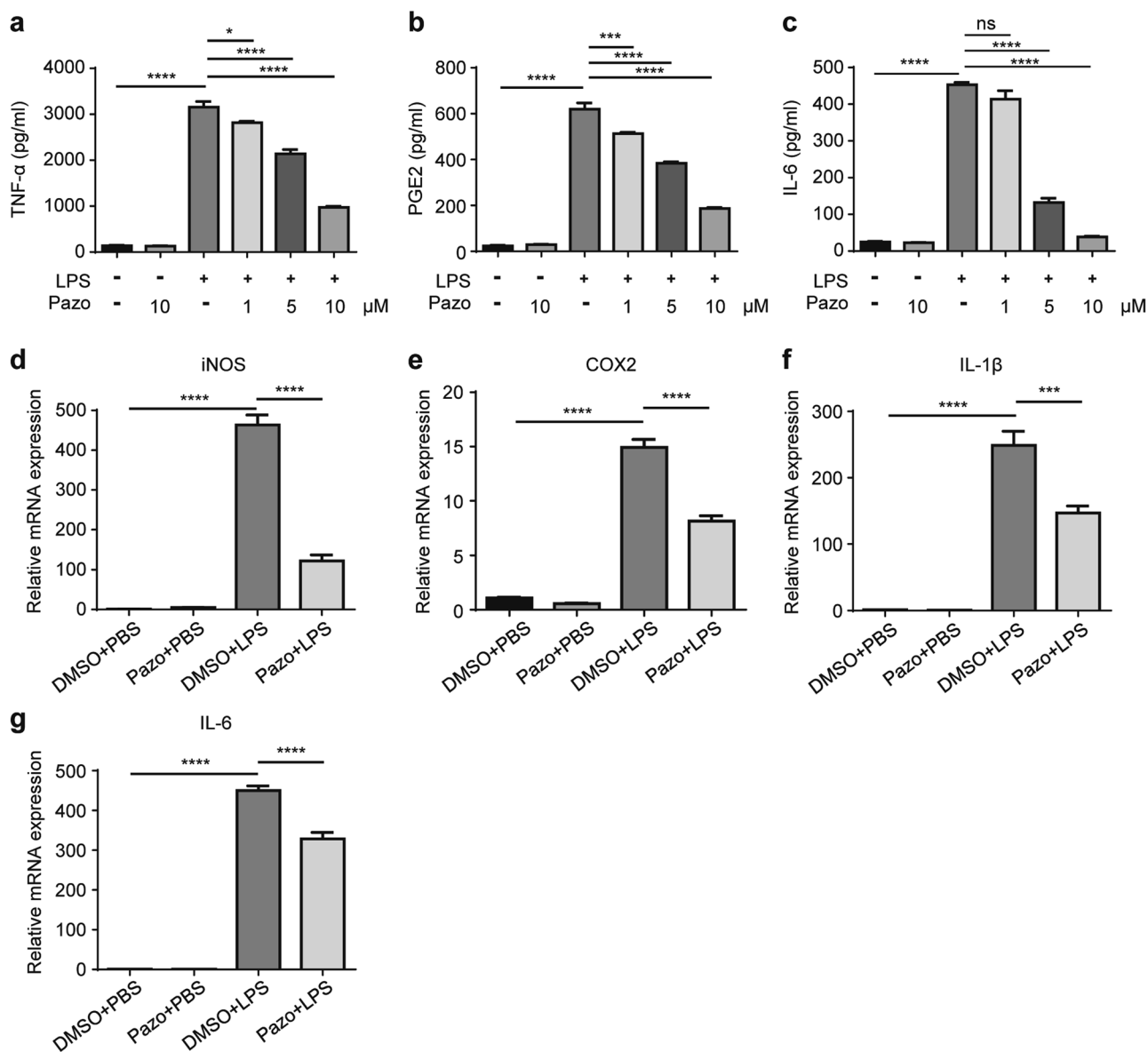


Fig. 3 Pazopanib inhibits the transcription of proinflammatory factors. a–c BV2 cells were pretreated with pazopanib (0, 1, 5, 10 μM) or DMSO for 4 h and then exposed to LPS (1 μg/mL) or PBS for 20 h. The levels of the proinflammatory factors TNF-α (a), PGE2 (b) and IL-6 (c) were measured using ELISA. The values are presented as the mean ± SEM from three independent experiments. **P* < 0.05, *****P* < 0.0001, ns no significant difference vs LPS group, one-way ANOVA followed by Dunnett's multiple-comparisons test. d–g BV2 cells were treated with pazopanib (5 μM) for 4 h or DMSO followed by LPS treatment for 12 h, and total RNA was collected to measure the mRNA levels of iNOS (d), COX2 (e), IL-1β (f), and IL-6 (g) using qPCR assays. The values are presented as the mean ± SEM from three independent experiments. *****P* < 0.0001, ******P* < 0.00001, one-way ANOVA followed by Dunnett's multiple-comparisons test.

suggest that pazopanib attenuates the activation of LPS-induced microglial activation via the MEK4-JNK-AP-1 pathway.

Pazopanib suppressed microglia-mediated MES23.5 cell death
Since we have shown that pazopanib has inhibitory effects on microglial activation, we wondered whether it could attenuate the neurotoxicity of hyperactive microglia to neurons. We performed a microglial conditioned medium (MCM) assay to identify the toxicity of MCM to neurons (Fig. 6a). Using PI staining, MES23.5 cell death was observed when the neurons were exposed to MCM from primary microglia that were treated with LPS (Fig. 6b, c). However, treatment with pazopanib significantly decreased the toxicity of MCM from microglia that were treated with LPS (Fig. 6b, c). Similar results were obtained using LDH assays (Fig. 6d). In addition, less cleavage of caspase-3 was detected in MES23.5 cells

that were exposed to MCM from LPS-stimulated primary microglia with pazopanib treatment than those without pazopanib treatment (Fig. 6e, f). Thus, our data suggest that pazopanib can suppress microglia-mediated neuronal toxicity.

Pazopanib inhibits neuroinflammation and protects dopaminergic neurons in LPS-stimulated mice

Since we identified the inhibitory effects of pazopanib on microglial activation in vitro, we wondered whether pazopanib could suppress glia-mediated DA neuronal loss in vivo. C57BL/6J mice were administered pazopanib with intraperitoneal injections and received a stereotaxic injection of LPS into the substantia nigra (Fig. 7a). No significant weight changes in the animals were observed at the doses that were administered to the animals (Fig. S3). We evaluated fine motor coordination using several behavioral tests, including the pole

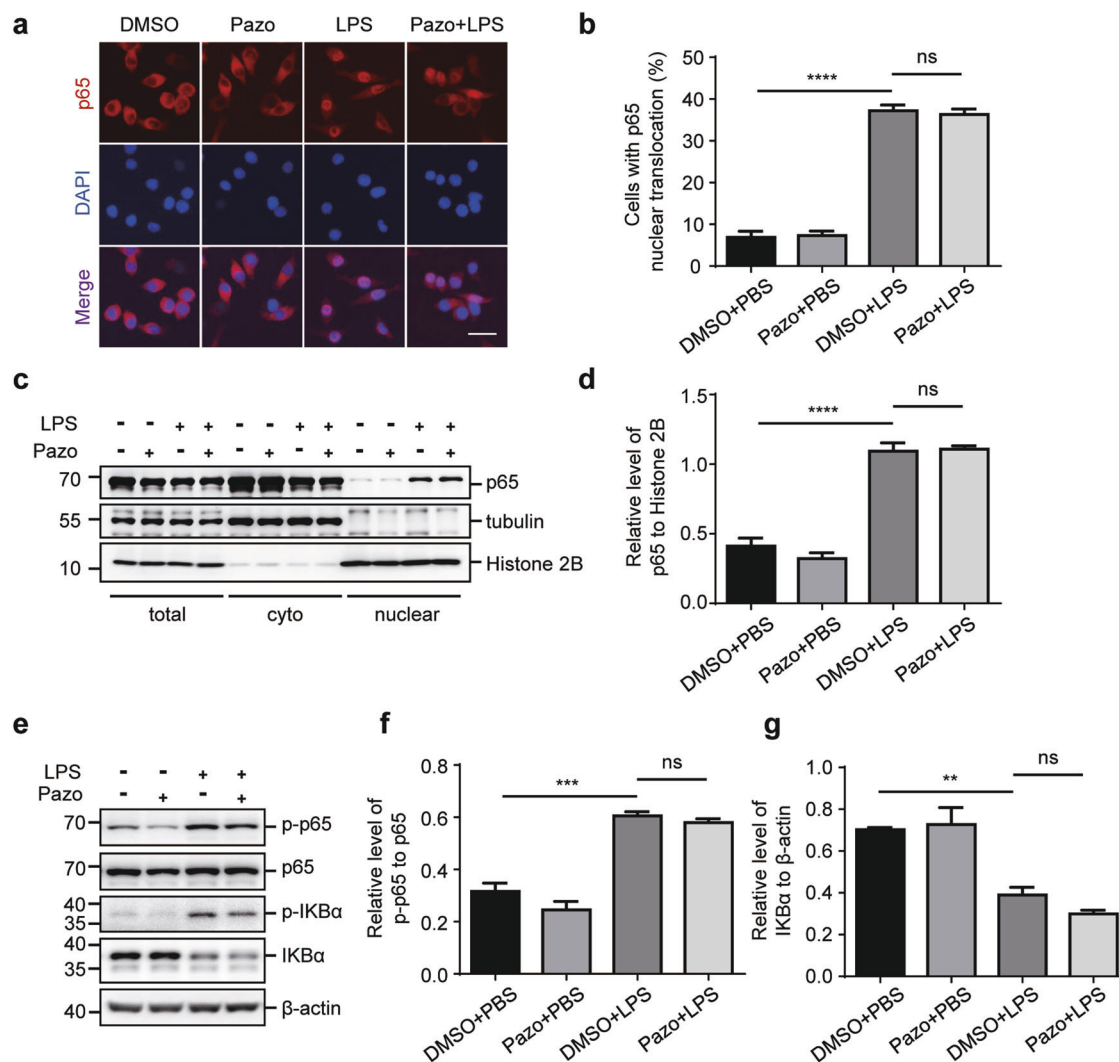


Fig. 4 The anti-inflammatory effect of pazopanib is independent of the NF- κ B pathway. **a, b** BV2 cells were treated with pazopanib (5 μ M) for 4 h and then exposed to LPS (1 μ g) for 15 min. After the treatment, cells were fixed and labeled with anti-p65 antibodies (red), while nuclei were labeled with DAPI (blue). The cells were imaged with a fluorescence microscope (**a**). Scale bar, 100 μ m. $n = 3$ per group. The cells with NF- κ B p65 nuclear translocation were quantified (**b**). The values are presented as the mean \pm SEM from three independent experiments. $****P < 0.001$, ns no significant difference, one-way ANOVA followed by Dunnett's multiple-comparisons test. **c, d** BV2 cells were treated as in (**a**) and then subjected to fractionation assays to separate into nuclear and cytoplasmic fractions. The p65 levels in different fractions were measured by immunoblot analyses. The quantification of the intensity of p65 relative to Histone 2B is shown (**d**). The values are presented as the mean \pm SEM from three independent experiments. $****P < 0.0001$, ns no significant difference, one-way ANOVA followed by Dunnett's multiple-comparisons test. **e, f** BV2 cells were treated as in A and then collected and subjected to immunoblot analyses with the indicated antibodies to measure the protein levels of p-p65, p65, p-IK β , IK β , and actin (**e**). The quantifications of the intensity of p-p65 to p65 or IK β to actin are shown (**f**) and (**g**). The values are presented as the mean \pm SEM from three independent experiments. $**P < 0.01$, $***P < 0.001$, ns no significant difference, one-way ANOVA followed by Dunnett's multiple-comparisons test.

test, beam walking test, rotarod test and open field test. LPS treatment significantly impaired the performance of the model mice in all behavioral tests. However, pazopanib pretreatment obviously improved the performance in LPS-stimulated mice. Compared with the LPS-stimulated mice without pazopanib treatment, mice that were pretreated with pazopanib showed a preference for the central area in the open field test (Fig. 7b) and better balance ability in the beam walking test (Fig. 7c). Moreover, pazopanib pretreatment shortened the test time in the pole test of model mice and prolonged their latency time on the rotarod, suggesting an improvement in their motor coordination ability (Fig. 7d, e).

We further analyzed the expression of inflammatory factors using qPCR. LPS increased the mRNA levels of iNOS, COX2, TNF- α and IL-6 in the midbrain; however, pretreatment with pazopanib attenuated the LPS-induced expression of the abovementioned

inflammatory factors (Fig. 7f). Similarly, LPS stimulation increased the expression of proinflammatory factors in the SN. The ELISA results indicated that pretreatment with pazopanib rescued LPS-induced neuroinflammation in vivo (Fig. 7g). Furthermore, the abundance of GFAP and IBA1 in the midbrain was increased after LPS treatment (Fig. 7h, i). However, pretreatment with pazopanib attenuated the LPS-induced upregulation of GFAP and IBA1 (Fig. 7h, i), further suggesting that pazopanib represses LPS-induced glial activation and the production of inflammatory factors. In addition, pazopanib treatment attenuated LPS-induced loss of TH-positive neurons in the midbrain and the decrease in TH immunoreactivity in the striatum (Fig. 7j, k). Overall, the VEGFR-TKI pazopanib rescued the behavioral abilities and protected dopaminergic neurons in an LPS-induced PD mouse model by inhibiting neuroinflammation.

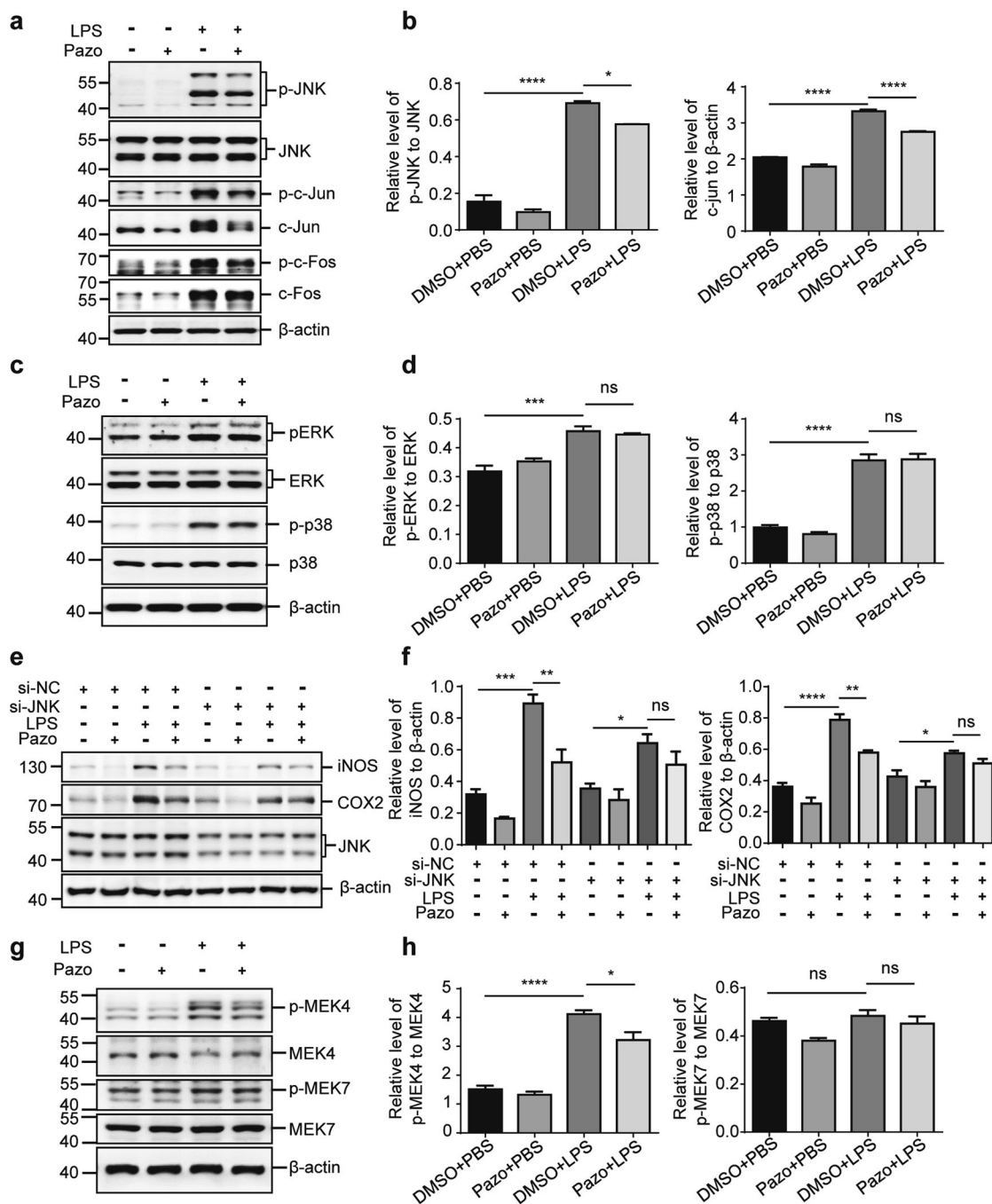


Fig. 5 Pazopanib alleviates LPS-induced inflammation through the AP-1 pathway. **a, b** BV2 cells were treated with pazopanib (5 μM) for 4 h and then exposed to LPS (1 μg) for 15 min. The protein levels of p-JNK, JNK, p-c-Jun, c-Jun, p-c-Fos, c-Fos, and β-actin were measured using immunoblot analyses (**a**). The quantifications of the intensity of p-JNK to JNK and c-Jun to β-actin are shown (**b**). The values are presented as the mean ± SEM from three independent experiments. **P* < 0.05, *****P* < 0.0001, one-way ANOVA followed by Dunnett's multiple-comparisons test. **c, d** BV2 cells were treated as in (**a**). The protein levels of p-ERK, ERK, p-p38, p38, and β-actin were measured using immunoblot analyses (**c**). The quantifications of the intensity of p-ERK to ERK and p-p38 to p38 are shown (**d**). The values are presented as the mean ± SEM from three independent experiments. ****P* < 0.001, *****P* < 0.0001, ns no significant difference, one-way ANOVA followed by Dunnett's multiple-comparisons test. **e, f** BV2 cells were treated as in (**a**). The protein levels of iNOS, COX2, JNK and β-actin were measured using immunoblot analyses (**e**). The quantifications of the intensity of iNOS to β-actin and COX2 to β-actin are shown (**f**). The values are presented as the mean ± SEM from three independent experiments. **P* < 0.05, ***P* < 0.01, ****P* < 0.001, *****P* < 0.0001, ns no significant difference, one-way ANOVA followed by Dunnett's multiple-comparisons test. **g, h** BV2 cells were treated as in (**a**). The protein levels of p-MEK4, MEK4, p-MEK7, MEK7, and β-actin were measured using immunoblot analyses (**g**). The quantifications of the intensity of p-MEK4 to MEK4 and p-MEK7 to MEK7 are shown (**h**). The values are presented as the mean ± SEM from three independent experiments. **P* < 0.05, *****P* < 0.0001, ns no significant difference, one-way ANOVA followed by Dunnett's multiple-comparisons test.

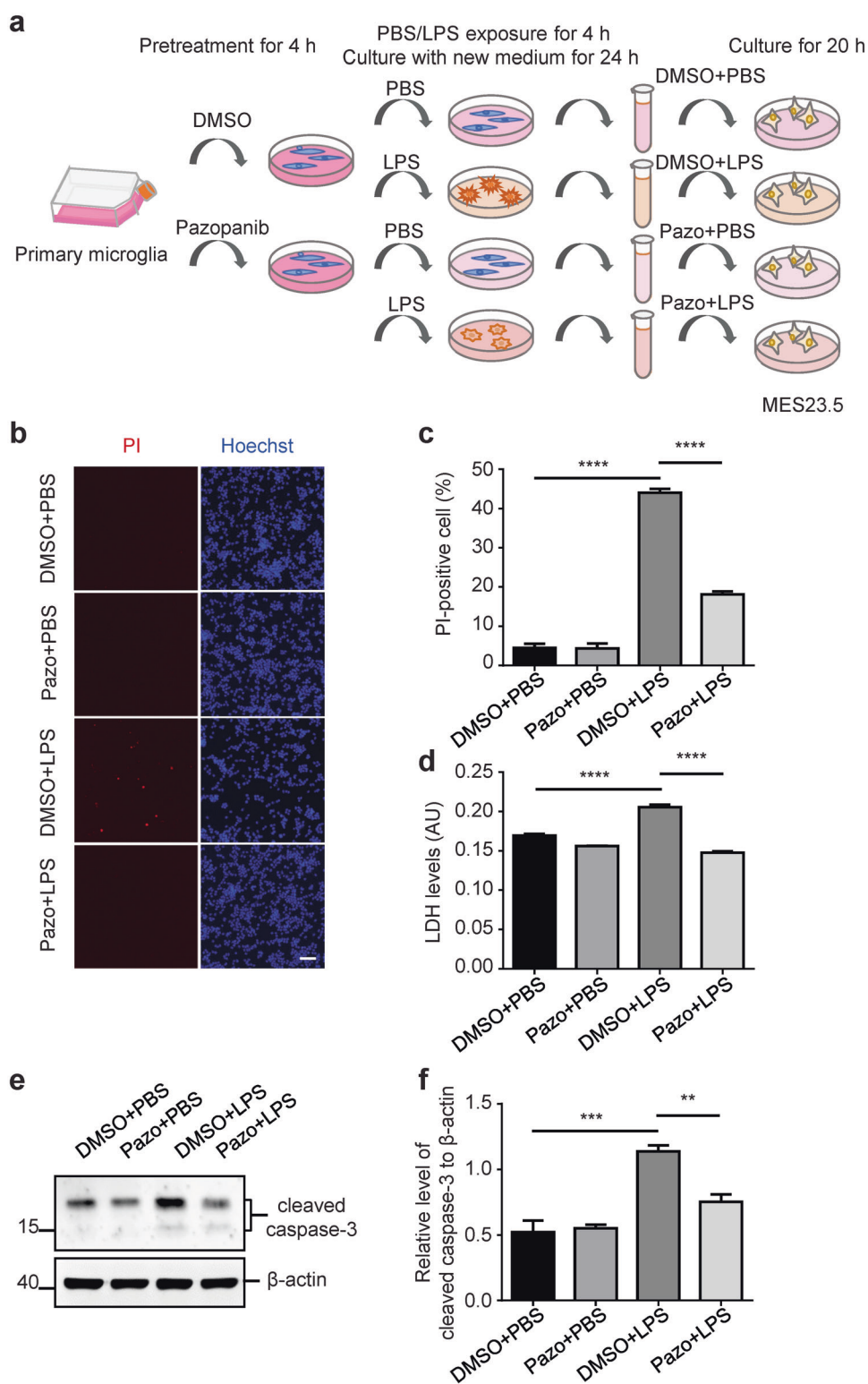
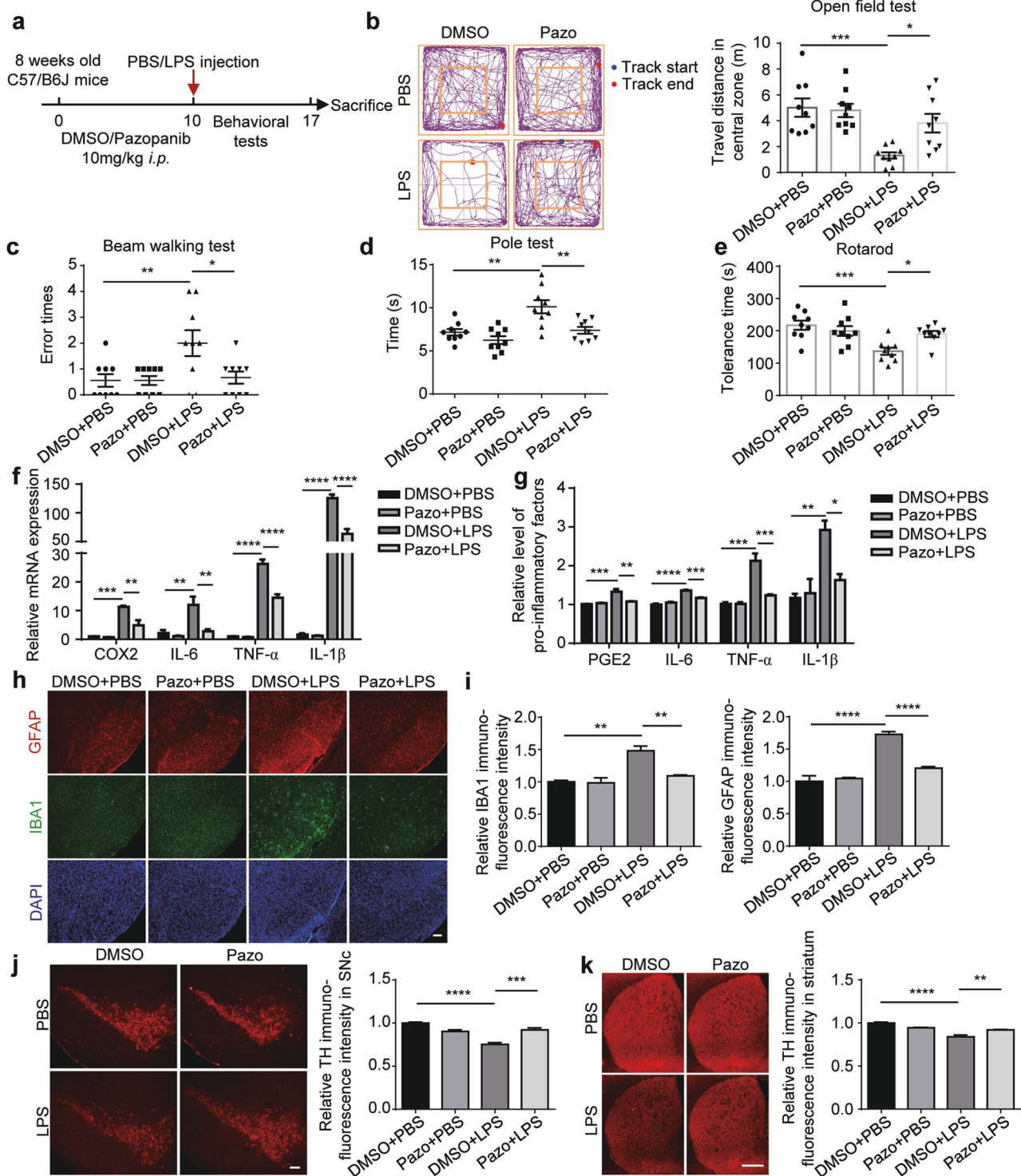


Fig. 6 Pazopanib suppressed microglia-mediated MES23.5 cell death. **a** Schematic diagram of the MCM assay. **b, c** MES23.5 cells were cultured with various M-CM for 24 h and then incubated with propidium iodide (PI) and Hoechst to detect the cell states (**b**). Scale bar, 100 μ m. $n = 3$ per group. The PI-positive cells were counted and quantified with cell numbers marked with Hoechst (**c**). The values are presented as the mean \pm SEM from three independent experiments. **** $P < 0.0001$, one-way ANOVA followed by Dunnett's multiple-comparisons test. **d** MES23.5 cells were treated as in (**b**). The culture media were collected to detect LDH release. The values are presented as the mean \pm SEM from three independent experiments. **** $P < 0.0001$, one-way ANOVA followed by Dunnett's multiple-comparisons test. **e, f** MES23.5 cells were treated as in (**b**). The cells were collected and subjected to immunoblot analyses using the indicated antibodies to measure the protein levels of cleaved caspase-3 and β -actin (**e**). The quantification of the intensity of cleaved caspase-3 relative to β -actin is shown (**f**). The values are presented as the mean \pm SEM from three independent experiments. ** $P < 0.01$, *** $P < 0.001$, one-way ANOVA followed by Dunnett's multiple-comparisons test.



DISCUSSION

Neuroinflammation is a common pathological feature in neurodegenerative diseases that occurs in the early stage and accelerates these diseases [41, 42]. Microglial activation occurs at the early stage of PD in living patients [43]. In PD patients who accept a transplantation of fetal mesencephalic tissue into the striatum, the activation of microglia occurs as early as 18 months after transplantation; however, pathogenic α -syn aggregates are present in the grafts until 14–16 years after transplantation [11], further suggesting that microglial activation is an early event of

PD. Thus, compounds/drugs that target hyperactivated microglia to attenuate microglia-mediated neuronal damage may benefit neuronal survival [44]. Due to the long time and very high cost for drug development, drug repositioning that uses an existing drug for a new medication has been considered by scientists in PD and neurodegenerative disease research to target either disease-related molecules [45] or neuroinflammation [46, 47]. In the present study, we screened an FDA-approved drug library for identifying anti-inflammatory candidates. Using TNF- α as an indicator, we identified that several categories of drugs have

Fig. 7 Pazopanib inhibits in vivo neuroinflammation and protects dopaminergic neurons. **a** Animal experimental procedure diagram. C57BL/6J mice were treated with solvent or pazopanib (10 mg/kg; i.p.) once daily for 10 days, followed by stereotactic injection with PBS or LPS (4 µg). Mice were sacrificed 7 days after LPS treatment. **b–e** The behavioral tests were conducted every day starting from day 12. $n = 9$ per group. **b** The open field test was monitored for 15 min, and the representative examples of the movement paths of the four groups of mice are shown in the left panel. The travel distance in the central area of the four groups of mice in the open field test is shown in the right panel. The values are presented as the mean \pm SEM. $*P < 0.05$, $***P < 0.001$, one-way ANOVA followed by Dunnett's multiple-comparisons test. **c** Number of footslips in the beam walking test. The values are presented as the mean \pm SEM. $*P < 0.05$, $***P < 0.01$, one-way ANOVA followed by Dunnett's multiple-comparisons test. **d** Climbing time on pole test. The values are presented as the mean \pm SEM. $**P < 0.01$, one-way ANOVA followed by Dunnett's multiple-comparisons test. **e** Latencies to fall from the accelerated rotating beams in the rotarod test. The values are presented as the mean \pm SEM. $*P < 0.05$, $***P < 0.001$, one-way ANOVA followed by Dunnett's multiple-comparisons test. **f** The relative mRNA levels of the proinflammatory factors COX2, IL-6, TNF- α and IL-1 β in the SNc from mice treated with DMSO or pazopanib after challenge with PBS or LPS. $n = 3$ per group. The values are presented as the mean \pm SEM. $**P < 0.01$, $***P < 0.001$, $****P < 0.0001$, one-way ANOVA followed by Dunnett's multiple-comparisons test. **g** ELISA of PGE2, IL-6, TNF- α and IL-1 β in the SNc from mice treated with DMSO or pazopanib after challenge with PBS or LPS. $n = 3$ per group. The values are presented as the mean \pm SEM. $*P < 0.05$, $**P < 0.01$, $****P < 0.0001$, one-way ANOVA followed by Dunnett's multiple-comparisons test. **h, i** The midbrain slices were subjected to immunohistochemical staining using anti-IBA1 and anti-GFAP antibodies. Scale bar, 100 µm. $n = 3$ per group. The relative fluorescence intensity of IBA1 and GFAP is shown (i). The values are presented as the mean \pm SEM from three independent experiments. $**P < 0.01$, $****P < 0.0001$, one-way ANOVA followed by Dunnett's multiple-comparisons test. **j** The midbrain slices were subjected to immunohistochemical staining using an anti-tyrosine hydroxylase (TH) antibody. The relative fluorescence intensity of TH is shown in the right panel. Scale bar, 100 µm. $n = 3$ per group. $***P < 0.001$, $****P < 0.0001$, one-way ANOVA followed by Dunnett's multiple-comparisons test. **k** The striatum slices were subjected to immunohistochemical staining using the TH antibody. The relative fluorescence intensity of TH is shown in the right panel. Scale bar, 100 µm. $n = 3$ per group. $**P < 0.01$, $****P < 0.0001$, one-way ANOVA followed by Dunnett's multiple-comparisons test.

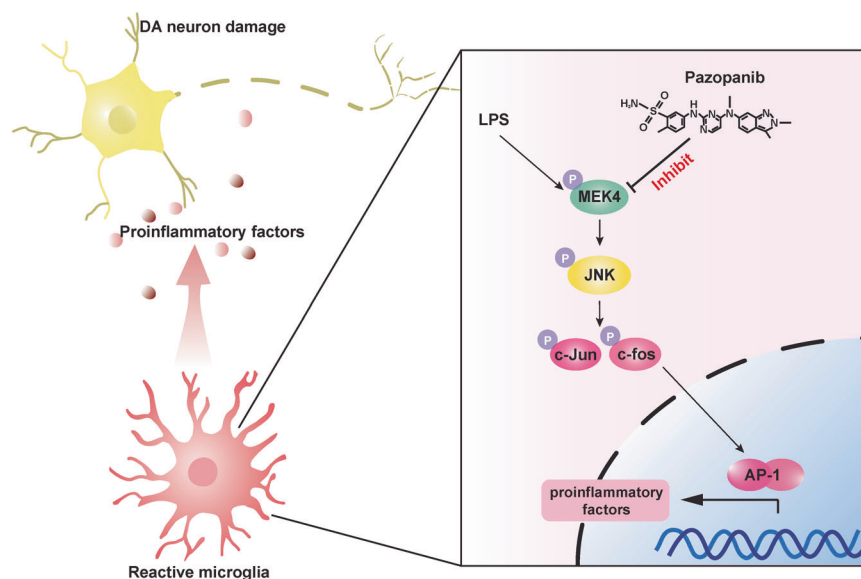


Fig. 8 Pazopanib alleviates LPS-induced inflammation through the MEK4-JNK-AP-1 pathway. A schematic diagram shows our small molecule compound library screening, and the VEGFR inhibitor pazopanib inhibits microglial hyperactivation and protects dopaminergic neurons from neuroinflammation-induced cell death in vitro and in vivo. Pazopanib alleviates LPS-induced neuroinflammation by inhibiting the MEK4-JNK-AP-1 pathway.

inhibitory effects on LPS-induced microglial activation, which target PI3K/AKT/mTOR, VEGFR, MEK, and other signaling pathways. Due to the emerging critical roles of tyrosine kinases in neuroimmune regulation, we focused on VEGFR inhibitor candidates.

Increasing evidence has shown that the tyrosine kinase system is involved in many neurological diseases, including neurodegenerative diseases, stroke, epilepsy, and spinal cord injury, and corresponding TKIs also show neuronal protection [48, 49]. It has been well documented that c-Abl inhibitors (nilotinib, bosutinib, radotinib), as well as Bruton's tyrosine kinase (BTK) inhibitor (ibrutinib), can mitigate the deposition of pathogenic proteins and protect neurons in animal models of AD, PD, and ALS, respectively [50–54]. These reports support our search for new applications of tyrosine kinase inhibitors.

We characterized the universal anti-inflammatory effects of VEGFR-TKIs, some of which are supported by previous studies [55–57]. Sorafenib was the first reported TKI that reduced AD pathology by reducing neuroinflammation by inhibiting NF- κ B

signaling [58]. A recent study showed that sorafenib also suppressed AKT/p38 and STAT3 in AD murine models [55]. Moreover, imatinib and sorafenib were reported to inhibit platelet-derived growth factor (PDGFR)-mediated astrocyte proliferation and LPS-induced macrophage TNF- α production [57]. In addition, regorafenib also rescued neuroinflammation in AD murine models by inhibiting the AKT-STAT3 pathway [56]. Here, we found that pazopanib is more effective in anti-neuroinflammation with lower toxicity in vitro and in vivo. High VEGF-A was observed in both cerebrospinal fluid (CSF) and blood in AD and PD patients and was positively correlated with the degree of cognitive impairment [59, 60]. In addition, microglial VEGF-B was proven to activate VEGFR in astrocytes, which worsens neuroinflammation [61]. Considering pathological changes in VEGF ligands together with the effective therapy of VEGFR-TKIs, we hypothesized that the activation of VEGF-A/B-VEGFR may be involved in neuroinflammatory responses [62, 63].

The NF- κ B pathway and the AP-1 pathway are classic signaling pathways that mediate the expression of proinflammatory factors

induced by LPS, which can be regulated by MAPK cascades [64, 65]. MAPK subfamilies consist of three core kinases, including ERK, JNK, and p38, which respond to immune stimulations via different pathways [65–67]. All MAPK antagonists have been suggested to reduce the production of microglial proinflammatory factors as well as ROS, which decreases the neurotoxicity of MCM [68]. Among them, the activation of JNK kinase is mainly regulated by the upstream kinases MEK4 and MEK7 [69, 70]. Inhibition of MEK4/7 pharmacologically with antagonists or genetically with gene ablation effectively suppresses downstream JNK signals and prevents proinflammatory phenotypes in macrophages and microglia [70–73]. In our observation, pazopanib inhibited LPS-induced MEK4-JNK-AP-1 axis activation in microglia. Pazopanib decreases LPS-induced MEK4 phosphorylation. As pazopanib is a potent MEK4 inhibitor with high affinity [74], it further suggests that pazopanib may repress MEK4 activation to alleviate LPS-induced microglial activation.

In conclusion, pazopanib suppresses MEK4 phosphorylation and subsequent JNK activation. The inhibition of the MEK4-JNK-AP-1 axis decreases LPS-induced microglial activation, which decreases the production of proinflammatory factors that are toxic to neurons (Fig. 8). Thus, our study provides a new strategy for the drug repositioning of VEGFR-TKIs, especially pazopanib, in neuroinflammation therapy.

AUTHOR CONTRIBUTIONS

HYS and GHW designed the study. HYS performed most of the experiments. JW, RW, SZ, and HX performed some of the biochemical and cellular experiments. XJL, HGR, and EK analyzed the data. HYS drafted the manuscript, and GHW revised the manuscript. All authors read and approved the manuscript.

FUNDING

This work was supported by the National Natural Science Foundation of China (No. 32271039, 32070970, and 31970966), the Joint Program RFBR-BRICS (No. 17-54-80006) and a Project Funded by the Priority Academic Program Development of Jiangsu Higher Education Institutions.

ADDITIONAL INFORMATION

Supplementary information The online version contains supplementary material available at <https://doi.org/10.1038/s41401-022-01030-1>.

Competing interests: The authors declare no competing interests.

REFERENCES

- Aarsland D, Batzu L, Halliday GM, Geurtsen GJ, Ballard C, Ray Chaudhuri K, et al. Parkinson disease-associated cognitive impairment. *Nat Rev Dis Prim*. 2021;7:47.
- Collaborators GBPsD. Global, regional, and national burden of Parkinson's disease, 1990–2016: a systematic analysis for the Global Burden of Disease Study 2016. *Lancet Neurol*. 2018;17:939–53.
- Lindqvist D, Hall S, Surova Y, Nielsen HM, Janelidze S, Brundin L, et al. Cerebrospinal fluid inflammatory markers in Parkinson's disease—associations with depression, fatigue, and cognitive impairment. *Brain Behav Immun*. 2013;33:183–9.
- Cheng J, Liao Y, Dong Y, Hu H, Yang N, Kong X, et al. Microglial autophagy defect causes parkinson disease-like symptoms by accelerating inflammasome activation in mice. *Autophagy*. 2020;16:2193–205.
- Mittal S, Bjornevik K, Im DS, Flierl A, Dong X, Locascio JJ, et al. beta2-Adrenoreceptor is a regulator of the alpha-synuclein gene driving risk of Parkinson's disease. *Science*. 2017;357:891–8.
- Lemos M, Venezia S, Refolo V, Heras-Garvin A, Schmidhuber S, Giese A, et al. Targeting alpha-synuclein by PD03 AFFITOPE(R) and Anle138b rescues neurodegenerative pathology in a model of multiple system atrophy: clinical relevance. *Transl Neurodegener*. 2020;9:38.
- Suresh SN, Chavalmame AK, Dj V, Yarreiphang H, Rai S, Paul A, et al. A novel autophagy modulator 6-Bio ameliorates SNCA/alpha-synuclein toxicity. *Autophagy*. 2017;13:1221–34.
- Issa AR, Sun J, Petitgas C, Mesquita A, Dulac A, Robin M, et al. The lysosomal membrane protein LAMP2A promotes autophagic flux and prevents SNCA-induced Parkinson disease-like symptoms in the *Drosophila* brain. *Autophagy*. 2018;14:1898–910.
- Mor DE, Sohrabi S, Kaletsky R, Keyes W, Tartici A, Kalia V, et al. Metformin rescues Parkinson's disease phenotypes caused by hyperactive mitochondria. *Proc Natl Acad Sci USA*. 2020;117:26438–47.
- Hebron ML, Lonskaya I, Olopade P, Selby ST, Pagan F, Moussa CE. Tyrosine kinase inhibition regulates early systemic immune changes and modulates the neuro-immune response in alpha-synucleinopathy. *J Clin Cell Immunol*. 2014;5:259.
- Olanow CW, Savolainen M, Chu Y, Halliday GM, Kordower JH. Temporal evolution of microglia and alpha-synuclein accumulation following foetal grafting in Parkinson's disease. *Brain*. 2019;142:1690–700.
- Garcia P, Jurgens-Wemheuer W, Uriarte Huarte O, Michelucci A, Masuch A, Brioschi S, et al. Neurodegeneration and neuroinflammation are linked, but independent of alpha-synuclein inclusions, in a seeding/spreading mouse model of Parkinson's disease. *Glia*. 2022;70:935–60.
- McFarthing K, Rafaloff G, Baptista MAS, Wyse RK, Stott SRW. Parkinson's disease drug therapies in the clinical trial pipeline: 2021 update. *J Parkinsons Dis*. 2021;11:891–903.
- Badanjak K, Fixemer S, Smajic S, Skupin A, Grunewald A. The contribution of microglia to neuroinflammation in Parkinson's disease. *Int J Mol Sci*. 2021;22:4647.
- Lempriere S. Age-related microglial activation accelerated in AD. *Nat Rev Neurol*. 2019;15:369.
- Kim BW, Koppula S, Kumar H, Park JY, Kim IW, More SV, et al. alpha-Asarone attenuates microglia-mediated neuroinflammation by inhibiting NF kappa B activation and mitigates MPTP-induced behavioral deficits in a mouse model of Parkinson's disease. *Neuropharmacology*. 2015;97:46–57.
- More S, Choi DK. Neuroprotective role of Atractylenolide-I in an in vitro and in vivo model of Parkinson's disease. *Nutrients*. 2017;9:451.
- Wang GQ, Li DD, Huang C, Lu DS, Zhang C, Zhou SY, et al. Icariin reduces dopaminergic neuronal loss and microglia-mediated inflammation in vivo and in vitro. *Front Mol Neurosci*. 2017;10:441.
- Chen H, Zhang SM, Hernan MA, Schwarzschild MA, Willett WC, Colditz GA, et al. Nonsteroidal anti-inflammatory drugs and the risk of Parkinson disease. *Arch Neurol*. 2003;60:1059–64.
- Gagne JJ, Power MC. Anti-inflammatory drugs and risk of Parkinson disease: a meta-analysis. *Neurology*. 2010;74:995–1002.
- Guo CH, Cao T, Zheng LT, Waddington JL, Zhen XC. Development and characterization of an inducible Dicer conditional knockout mouse model of Parkinson's disease: validation of the antiparkinsonian effects of a sigma-1 receptor agonist and dihydromyricetin. *Acta Pharmacol Sin*. 2020;41:499–507.
- Ren ZX, Zhao YF, Cao T, Zhen XC. Dihydromyricetin protects neurons in an MPTP-induced model of Parkinson's disease by suppressing glycogen synthase kinase-3 beta activity. *Acta Pharmacol Sin*. 2016;37:1315–24.
- Sun J, Li H, Jin Y, Yu J, Mao S, Su KP, et al. Probiotic *Clostridium butyricum* ameliorated motor deficits in a mouse model of Parkinson's disease via gut microbiota-GLP-1 pathway. *Brain Behav Immun*. 2021;91:703–15.
- Hao Z, Liu L, Tao Z, Wang R, Ren H, Sun H, et al. Motor dysfunction and neurodegeneration in a C9orf72 mouse line expressing poly-PR. *Nat Commun*. 2019;10:2906.
- Cao M, Chen F, Xie N, Cao MY, Chen P, Lou Q, et al. c-Jun N-terminal kinases differentially regulate TNF- and TLRs-mediated necroptosis through their kinase-dependent and -independent activities. *Cell Death Dis*. 2018;9:1140.
- Yu YX, Li YP, Gao F, Hu QS, Zhang Y, Chen D, et al. Vitamin K2 suppresses rotenone-induced microglial activation in vitro. *Acta Pharmacol Sin*. 2016;37:1178–89.
- Guo DK, Zhu Y, Sun HY, Xu XY, Zhang S, Hao ZB, et al. Pharmacological activation of REV-ERBalpha represses LPS-induced microglial activation through the NF-kappaB pathway. *Acta Pharmacol Sin*. 2019;40:26–34.
- Han CJ, Zheng JY, Sun L, Yang HC, Cao ZQ, Zhang XH, et al. The oncometabolite 2-hydroxyglutarate inhibits microglial activation via the AMPK/mTOR/NF-kappaB pathway. *Acta Pharmacol Sin*. 2019;40:1292–302.
- Gu C, Hu Q, Wu J, Mu C, Ren H, Liu CF, et al. P7C3 inhibits LPS-induced microglial activation to protect dopaminergic neurons against inflammatory factor-induced cell death in vitro and in vivo. *Front Cell Neurosci*. 2018;12:400.
- Fang J, She J, Lin F, Wu JC, Han R, Sheng R, et al. RRx-001 exerts neuroprotection against LPS-induced microglia activation and neuroinflammation through disturbing the TLR4 pathway. *Front Pharmacol*. 2022;13:889383.
- Yan XL, Xu FY, Ji JJ, Song P, Pei YQ, He MJ, et al. Activation of UCP2 by anethole trithione suppresses neuroinflammation after intracerebral hemorrhage. *Acta Pharmacol Sin*. 2022;43:811–28.
- Lee HG, Wheeler MA, Quintana FJ. Function and therapeutic value of astrocytes in neurological diseases. *Nat Rev Drug Discov*. 2022;21:339–58.

33. Liddel SA, Guttenplan KA, Clarke LE, Bennett FC, Bohlen CJ, Schirmer L, et al. Neurotoxic reactive astrocytes are induced by activated microglia. *Nature*. 2017;541:481–7.
34. Limvorasak S, Posadas EM. Pazopanib: therapeutic developments. *Expert Opin Pharmacother*. 2009;10:3091–102.
35. Karin M, Cao Y, Greten FR, Li ZW. NF-kappaB in cancer: from innocent bystander to major culprit. *Nat Rev Cancer*. 2002;2:301–10.
36. Backert S, Naumann M. What a disorder: proinflammatory signaling pathways induced by *Helicobacter pylori*. *Trends Microbiol*. 2010;18:479–86.
37. Yu H, Pardoll D, Jove R. STATs in cancer inflammation and immunity: a leading role for STAT3. *Nat Rev Cancer*. 2009;9:798–809.
38. Nagamoto-Combs K, Combs CK. Microglial phenotype is regulated by activity of the transcription factor, NFAT (nuclear factor of activated T cells). *J Neurosci*. 2010;30:9641–6.
39. O'Neill LA, Golenbock D, Bowie AG. The history of Toll-like receptors—redefining innate immunity. *Nat Rev Immunol*. 2013;13:453–60.
40. Dainichi T, Matsumoto R, Mostafa A, Kabashima K. Immune control by TRAF6-Mediated pathways of epithelial cells in the EIME (Epithelial Immune Micro-environment). *Front Immunol*. 2019;10:1107.
41. Colonna M, Brioschi S. Neuroinflammation and neurodegeneration in human brain at single-cell resolution. *Nat Rev Immunol*. 2020;20:81–2.
42. Beers DR, Appel SH. Immune dysregulation in amyotrophic lateral sclerosis: mechanisms and emerging therapies. *Lancet Neurol*. 2019;18:211–20.
43. Gerhard A, Pavese N, Hotton G, Turkheimer F, Es M, Hammers A, et al. In vivo imaging of microglial activation with [¹¹C](R)-PK11195 PET in idiopathic Parkinson's disease. *Neurobiol Dis*. 2006;21:404–12.
44. Zhen XC, Chu HY. Emerging novel approaches to drug research and diagnosis of Parkinson's disease. *Acta Pharmacol Sin*. 2020;41:439–41.
45. Fletcher EJR, Kaminski T, Williams G, Duty S. Drug repurposing strategies of relevance for Parkinson's disease. *Pharm Res Perspect*. 2021;9:e00841.
46. Arbo BD, Schimith LE, Goulart Dos Santos M, Hort MA. Repositioning and development of new treatments for neurodegenerative diseases: Focus on neuroinflammation. *Eur J Pharmacol*. 2022;919:174800.
47. Zhang G, Chen S, Jia J, Liu C, Wang W, Zhang H, et al. Development and evaluation of novel metformin derivative metformin threonate for brain Ischemia treatment. *Front Pharmacol*. 2022;13:879690.
48. Janelidze S, Mattsson N, Stomrud E, Lindberg O, Palmqvist S, Zetterberg H, et al. CSF biomarkers of neuroinflammation and cerebrovascular dysfunction in early Alzheimer disease. *Neurology*. 2018;91:e867–e77.
49. Xu Z, Han K, Chen J, Wang C, Dong Y, Yu M, et al. Vascular endothelial growth factor is neuroprotective against ischemic brain injury by inhibiting scavenger receptor A expression on microglia. *J Neurochem*. 2017;142:700–9.
50. Lonskaya I, Hebron ML, Selby ST, Turner RS, Moussa CE. Nilotinib and bosutinib modulate pre-plaque alterations of blood immune markers and neuroinflammation in Alzheimer's disease models. *Neuroscience*. 2015;304:316–27.
51. Palomo V, Nozal V, Rojas-Prats E, Gil C, Martinez A. Protein kinase inhibitors for amyotrophic lateral sclerosis therapy. *Br J Pharmacol*. 2021;178:1316–35.
52. Lee S, Kim S, Park YJ, Yun SP, Kwon SH, Kim D, et al. The c-Abl inhibitor, Radotinib HCl, is neuroprotective in a preclinical Parkinson's disease mouse model. *Hum Mol Genet*. 2018;27:2344–56.
53. Imamura K, Izumi Y, Watanabe A, Tsukita K, Woltjen K, Yamamoto T, et al. The Src/c-Abl pathway is a potential therapeutic target in amyotrophic lateral sclerosis. *Sci Transl Med*. 2017;9:eaaf3962.
54. Lee HJ, Jeon SG, Kim J, Kang RJ, Kim SM, Han KM, et al. Ibrutinib modulates Abeta/tau pathology, neuroinflammation, and cognitive function in mouse models of Alzheimer's disease. *Aging Cell*. 2021;20:e13332.
55. Kim J, Park JH, Park SK, Hoe HS. Sorafenib modulates the LPS- and abeta-induced neuroinflammatory response in cells, wild-type mice, and 5xFAD mice. *Front Immunol*. 2021;12:684344.
56. Han KM, Kang RJ, Jeon H, Lee HJ, Lee JS, Park H, et al. Regorafenib regulates AD pathology, neuroinflammation, and dendritic spinogenesis in cells and a mouse model of AD. *Cells*. 2020;9:1655.
57. Crespo O, Kang SC, Daneman R, Lindstrom TM, Ho PP, Sobel RA, et al. Tyrosine kinase inhibitors ameliorate autoimmune encephalomyelitis in a mouse model of multiple sclerosis. *J Clin Immunol*. 2011;31:1010–20.
58. Echeverria V, Burgess S, Gamble-George J, Zeitlin R, Lin X, Cao C, et al. Sorafenib inhibits nuclear factor kappa B, decreases inducible nitric oxide synthase and cyclooxygenase-2 expression, and restores working memory in APPswe mice. *Neuroscience*. 2009;162:1220–31.
59. Bowman GL, Dayon L, Kirkland R, Wojcik J, Peyratout G, Severin IC, et al. Blood-brain barrier breakdown, neuroinflammation, and cognitive decline in older adults. *Alzheimers Dement*. 2018;14:1640–50.
60. Janelidze S, Lindqvist D, Francardo V, Hall S, Zetterberg H, Blennow K, et al. Increased CSF biomarkers of angiogenesis in Parkinson disease. *Neurology*. 2015;85:1834–42.
61. Rothhammer V, Borucki DM, Tjon EC, Takenaka MC, Chao CC, Ardura-Fabregat A, et al. Microglial control of astrocytes in response to microbial metabolites. *Nature*. 2018;557:724–8.
62. Wekerle H. Brain inflammatory cascade controlled by gut-derived molecules. *Nature*. 2018;557:642–3.
63. Cirac A, Tsaktanis T, Beyer T, Linnerbauer M, Andlauer T, Grummel V, et al. The Aryl hydrocarbon receptor-dependent TGF-alpha/VEGF-B ratio correlates with disease subtype and prognosis in multiple sclerosis. *Neurol Neuroimmunol Neuroinflamm*. 2021;8:e1043.
64. Waetzig V, Czeloth K, Hidding U, Mielke K, Kanzow M, Brecht S, et al. c-Jun N-terminal kinases (JNKs) mediate pro-inflammatory actions of microglia. *Glia*. 2005;50:235–46.
65. Liu Z, Yao X, Sun B, Jiang W, Liao C, Dai X, et al. Pretreatment with kaempferol attenuates microglia-mediate neuroinflammation by inhibiting MAPKs-NF-kappaB signaling pathway and pyroptosis after secondary spinal cord injury. *Free Radic Biol Med*. 2021;168:142–54.
66. Wu B, Zhang S, Guo Z, Bi Y, Zhou M, Li P, et al. The TGF-beta superfamily cytokine Activin-A is induced during autoimmune neuroinflammation and drives pathogenic Th17 cell differentiation. *Immunity*. 2021;54:308–23 e6.
67. Zhang J, Liu Y, Zheng Y, Luo Y, Du Y, Zhao Y, et al. TREM-2-p38 MAPK signaling regulates neuroinflammation during chronic cerebral hypoperfusion combined with diabetes mellitus. *J Neuroinflammation*. 2020;17:2.
68. Plastira I, Bernhart E, Joshi L, Koyani CN, Strohmaier H, Reicher H, et al. MAPK signaling determines lysophosphatidic acid (LPA)-induced inflammation in microglia. *J Neuroinflammation*. 2020;17:127.
69. Caliz AD, Yoo HJ, Vertii A, Dolan AC, Tournier C, Davis RJ, et al. Mitogen kinase kinase (MKK7) controls cytokine production in vitro and in vivo in mice. *Int J Mol Sci*. 2021;22:9364.
70. Preston SP, Doerflinger M, Scott HW, Allison CC, Horton M, Cooney J, et al. The role of MKK4 in T-cell development and immunity to viral infections. *Immunol Cell Biol*. 2021;99:428–35.
71. Yu T, Wang Z, Jie W, Fu X, Li B, Xu H, et al. The kinase inhibitor BX795 suppresses the inflammatory response via multiple kinases. *Biochem Pharmacol*. 2020;174:113797.
72. Wang MJ, Huang HY, Chen WF, Chang HF, Kuo JS. Glycogen synthase kinase-3beta inactivation inhibits tumor necrosis factor-alpha production in microglia by modulating nuclear factor kappaB and MLK3/JNK signaling cascades. *J Neuroinflammation*. 2010;7:99.
73. Lee N, Heo YJ, Choi SE, Jeon JY, Han SJ, Kim DJ, et al. Anti-inflammatory effects of empagliflozin and gemigliptin on LPS-stimulated macrophage via the IKK/NF-kappaB, MKK7/JNK, and JAK2/STAT1 signalling pathways. *J Immunol Res*. 2021;2021:9944880.
74. Deibler KK, Mishra RK, Clutter MR, Antanasijevic A, Bergan R, Caffrey M, et al. A chemical probe strategy for interrogating inhibitor selectivity across the MEK kinase family. *ACS Chem Biol*. 2017;12:1245–56.

Springer Nature or its licensor (e.g. a society or other partner) holds exclusive rights to this article under a publishing agreement with the author(s) or other rightsholder(s); author self-archiving of the accepted manuscript version of this article is solely governed by the terms of such publishing agreement and applicable law.